ORIGINAL ARTICLE

Activated Carbon Doped with Silica and Nitrogen as Novel Adsorbent for Enhancing Adsorption Capacity of Cr(VI)

Ghada M. Mohamed[1] · Sohair A. Sayed Ahmed[1] · Nady A. Fathy[1]

Abstract

Due to the environmental concerns and the potential hazards and risks posed by chromium (VI), its removal from aquatic habitats has become a serious demand. In this paper, novel modifications were employed to increase the adsorption performance of Cr (VI) using activated carbon (AC) derived from sugarcane bagasse activated with phosphoric acid. AC was consequently modified with triethoxysilane propylamine and diethylene triamine as silica (Si) and nitrogen (N) sources, respectively. SEM-EDX, N_2 adsorption isotherms and FTIR analyses were performed to characterize the adsorbents. Equilibrium adsorption behavior of Cr(VI) ions with respect to varying in surface characteristics of resulting materials was investigated using Langmuir, Freundlich and Temkin isotherms. Kinetic and thermodynamic studies of Cr(VI) adsorption over AC, Si@AC and Si-N@AC were carried out. Freundlich model described the adsorption isotherm of AC and Si-N@AC severally, suggesting that the Cr(VI) removal was multi-layer adsorption. However, Langmuir model satisfied with adsorption of Cr (VI) over Si@AC. Pseudo-second order model fitted well the adsorption suggesting the chemical interaction. As a result of doping AC with Si and N, high adsorption capacities obtained at pH 2 and 30°C were to be 268 and 233 mg/g for Si@AC and Si-N@AC which are especially superior compared to others in literature.

Keywords Sugarcane bagasse · Activated carbon · Si and N-doping · Cr(VI) · Adsorption · Thermodynamics

1 Introduction

Wastewater from industries such as chrome plating, textiles, ceramics, photography, chrome leather tanning, metallurgy, and photoengraving has moderate to high levels of Cr(VI) compounds that exceed the regulation limit of 0.1 mg/L. Because Cr(VI) effluents causes lung cancer, ulcers, nasal septum perforations, and kidney damage in humans, thus these effluents must be remedied [1–5]. Toxic forms of Cr(VI) in wastewater are (CrO_2^{-4}) or ($HCrO_4^{-}$) species. Methods such as precipitation, electrochemical reduction, ion exchange, electrodeposition, membrane technology, and adsorption are currently used to remove chromium species from wastewater [4, 5]. However, adsorption remains one of the most cost-effective and widely used methods for eliminating harmful pollutants from wastewater. In particular, carbonaceous materials derived from agricultural wastes are the most widely used in adsorption process as adsorbents to provide simple, eco-friendly, valuable and less expensive treatment. Among these carbons, activated carbons (ACs) possess high specific surface area, the microporous character, and their surface chemical nature can exhibit good removal of Cr (VI) from aqueous solutions [6–14]. In addition, biomass wastes such as rutin [3], palm branch modified with surfactants [4] and extracellular polymeric substances [5] have been studied to decrease the cost of Cr (VI) elimination. However, the amount of Cr (VI) uptake by these biosorbents is still relatively low when compared to that removed by ACs materials [13, 14]. The internal porous structure of ACs possesses narrow micropores which hinder the diffusion of the metals onto its porous structure and thus can limit the removal of Cr(VI) anions.

Several strategies have been implemented in order to improve the properties of ACs in one of the most rapidly developing areas of environmental application, such as wastewater treatment. Several modification procedures

✉ Nady A. Fathy
    fathyna.77@hotmail.com

1   Physical Chemistry Department, Research Institute of
    Advanced Materials Technology and Mineral Resources,
    National Research Centre, 33 EL Buhouth St., P.O. 12622,
    Dokki, Cairo, Egypt

were used to ACs during or after their preparation in order to improve their ability to remove Cr(VI) with improved efficiency and regeneration. For example, earlier Aggarwal et al. [14] examined the efficiency removal of Cr(VI) using oxidized ACs with oxidizing agents and degassed ACs at elevated temperatures, concluding that the oxidation of the carbon surface enhances the amount of acidic carbon–oxygen surface groups which suppresses the adsorption of Cr(VI) whereas degassing eliminates these surface groups. In a very recent work, nitrogen (N)-doped porous carbon adsorbent derived from loofah sponge exhibited superior adsorption capacity of Cr(VI) reached to 227.3 mg/g [15], resulting in presence of N-containing functional groups with increasing electrostatic interactions between Cr(VI) species ($Cr_2O_7^{2-}$, CrO_4^{2-}, and $HCrO^{4-}$) and positively charged groups on AC surface. In the same concept, N-doped AC derived from steam activation of bean dreg precursors showed a high Cr(VI) adsorption capacity about 171.3 mg/g [16]. Moreover, such materials exhibited superior recyclability in Cr(VI) adsorption [15, 16]. Very lately, carbon-based nanostructures (CNSs) composed of carbon nanotubes and graphene sheets and derived from chemical vapor deposition of camphor and sugarcane bagasse waste were revealed efficient removal of Cr(VI) with a maximum adsorption capacity of 54 mg/g [17]. Where in case of chitosan grafted graphene oxide, superior adsorption for Cr(VI) of 104 mg/g was found [18]. However, this finding was still comparable to adsorption capacity of ACs [6–13]. Therefore, doping of ACs surface with N-containing functional groups is more active and efficient to ACs or CNSs individually; whether

those have low or high total surface area. After an extensive literature survey, we found that Cr(VI) removal from wastewater using triethoxysilane propylamine (TEPSA) as silica (Si) source and diethylene triamine (DETA) as nitrogen (N) source doped-activated carbon has not been investigated till now in detail. Recently, Biag et al. [19] prepared novel corrosion inhibitor from graphene oxide functionalized with DETA. An adsorbent of polyaniline/silica gel composite has been studied for removal of Cr(VI), and the maximum Cr(VI) ion adsorption capacity was found to be 63.41 mg/g [20], and silica gel with 4-acetyl-3-hydroxyaniline for adsorption of Cr(VI) was studied in another literature [21].

Therefore, the main objective of this research was to enhance the adsorption efficiency of AC prepared from sugarcane bagasse through its modifying with triethoxysilane propylamine (TEPSA) and diethylene triamine (DETA) reagents as silica and nitrogen sources, respectively. It is worth mentioning that this is the first work for designing new formulations of Si and Si-N doped surface of the prepared AC to exploring their adsorption capacities toward Cr (VI) removal as shown in Fig. 1. The morphology and surface compositions were identified by SEM-EDX (scanning electron microscopy coupled to an energy-dispersive X-ray spectroscopy), while functional groups on AC samples were determined using FTIR spectroscopy. Equilibrium adsorption behavior of Cr(VI) ions using Langmuir, Freundlich and Temkin isotherms as well as kinetic and thermodynamic studies of Cr(VI) adsorption were determined.

Fig. 1 Schematic diagram for modifying AC with TEPSA and DETA.
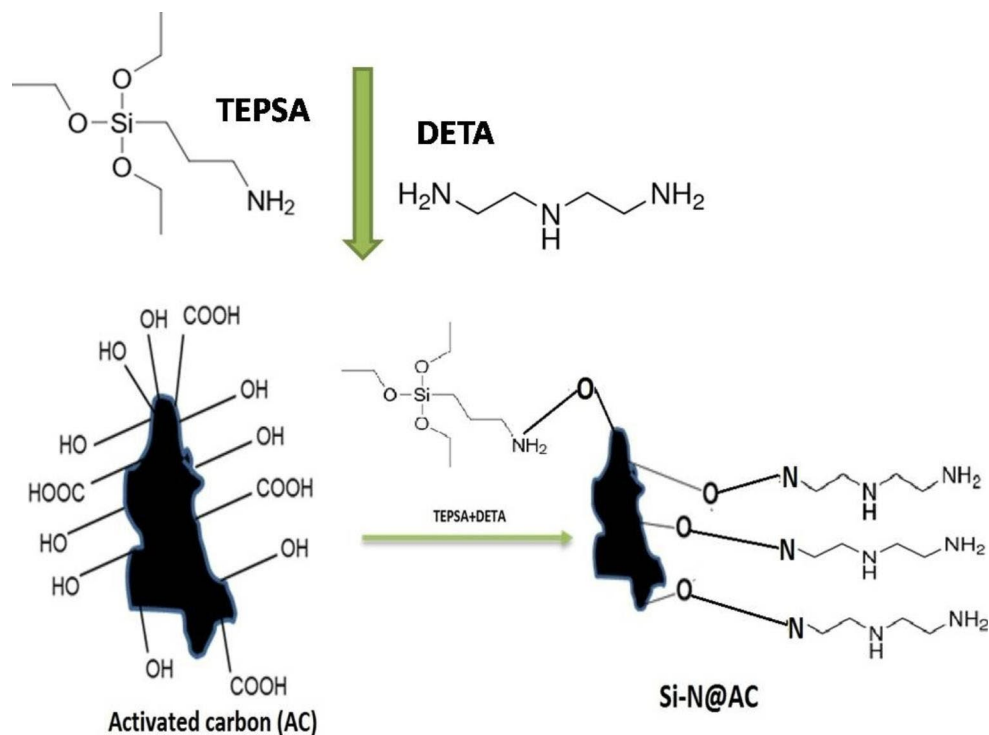
2 Materials and Methods

2.1 Materials

Ortho phosphoric acid (H_3PO_4, 85 wt%, $Mw = 98.0$ g/mol) was supplied from Rasayan (Turkey). Triethoxysilane propylamine [TESPA] or (3 Aminopropyl) triethoxysilane ($H_2N(CH_2)_3Si(OC_2H_5)_3$, $Mw = 221.37$ g/mol) was purchased from Sigma-Aldrich. Diethylene triamine [DETA] (($NH_2CH_2CH_2)_2NH$, $Mw = 103.17$ g/mol) was obtained from Thermo Scientific brand of ACROS Organics. TESPA and DETA were used as precursors for Si and N elements.

2.2 Preparation of Modified Activated Carbons

Crushed sugarcane bagasse pieces were dried at 100^oC overnight after washing with boiling water. Then, the sugarcane bagasse pieces were ground and carbonized in cylindrical stainless steel at 400^oC for 60 min under its own atmosphere to obtain char. Then, the char was impregnated with H_3PO_4 acid (50% v/v) and soaked for 48 h followed by filtration and drying. The obtained black char was then poured into a cylindrical seamless steel reactor with a tight lid, to prevent oxygen from entering the reactor. When the furnace temperature reached 500 °C under flowing N_2 gas, the reaction was continued at this degree for two hours. The obtained activated carbon was labelled as AC.

For modification process, 2 mL of TESPA was added to AC dispersed in 20 mL bi-distilled H_2O under stirring and heating at 50^oC. The obtained solid was separated from solution by filtration, washed thoroughly with bi-distilled water until the pH of filtrate becomes ~ 6, and dried at 80^oC overnight. The obtained sample was noted as Si@AC and weighted. The net weight in AC was increased about 15% after incorporation of Si particles. Third, About 2 g of AC was mixed with 1 mL of TESPA diluted to 20 mL of bi-distilled H_2O, heated to 50^oC under stirring for 1 h and then 1 mL of DETA was slowly added to mixture of AC and TESPA. After 2 h, 2 mL of DETA was slowly added to mixture of AC and TESPA and left overnight. The mixture was kept overnight without heating and stirring then followed by washing with bi-distilled H_2O until the pH of filtrate becomes ~ 6, and dried at 80^oC overnight. The resulted sample was noted as Si-N@AC.

2.3 Characterization of the Prepared Samples

The morphology and surface characteristics of the prepared samples were determined using scanning electron microscope (SEM, FEI Quanta FEG-250) combined with an energy-dispersive X-ray spectroscopy (EDX). Also, the textural properties such as Brunauer-Emmett-Teller (BET)

surface area (S_{BET}, m^2/g), total pore volume (V_P, cm^3/g) and average pore diameter (R_P, nm) were measured using nitrogen adsorption analysis at -196°C (BEL-Sorp-max, MicrotracBel Crop, Japan). Fourier transforms infrared spectroscopy (FTIR) spectra of samples were recorded by employing a KBr pressed disc technique (2 mg of sample and 98 mg of KBr) to give the main functional groups using FTIR 6500 spectrometer (JASCO, Japan) in the range of 400–4000 cm^{-1}.

2.4 Adsorption Measurements

To estimate the static adsorption behavior of Cr(VI) by the prepared carbon adsorbents, i.e. AC, Si@AC and Si-N@AC, the experiments under different conditions were accomplished. The effects of initial concentrations of Cr(VI) (20–100 mg/L), temperature of adsorption system (30–50 °C) and different contact time (0-180 min) on the adsorption performance were explored, respectively. The adsorption thermodynamic equation, kinetic equation and Van't Hoff equation of the adsorbed Cr(VI) using the tested samples were obtained by calculation.

2.5 Adsorption Calculations

After carrying out adsorption tests, the adsorbents were separated by filter paper, the residual concentrations of Cr(VI) solutions were determined according to the absorbance at the wavelength of 540 nm using a UV-Vis spectrophotometer (Shimadzu-PC2401, Japan). Percentage removal of Cr(VI) from synthetic solution (R%) using samples was calculated by using the following equation:

$$R\% = \frac{(C_0 - C_e)\ 100}{C_0} \qquad (1)$$

The amount of Cr(VI) ion adsorbed qe (mg/g) was calculated using this equation:

$$q_e = \frac{(C_0 - C_e)\ V}{m} \qquad (2)$$

The amount of Cr(VI) (q_t, mg/g) removed by the obtained nanohybrid at time t (min), was calculated by means of the expression below:

$$q_1 = \frac{(C_0 - C_e)\ V}{m} \qquad (3)$$

where C_0, C_e and C_t are the concentrations of Cr(VI) in aqueous solution (mg/L) at initial, equilibrium and definite time (t), V is the volume of the solution (L) and m is the mass of

adsorbent (g). The experimental data from this study were analyzed using the linear forms of three different models that are Freundlich, Langmuir and Temkin models [22, 23], to determine the equilibrium relationships as follows.

The Langmuir model describes monolayer adsorption on distinct adsorption sites that are localized. It assumes that all active sites are the same and symmetrical (homogenous). The linear form of Langmuir model is as indicated in Eq. (4) [22]:

$$\frac{1}{q_e} = \frac{1}{q_L} + \frac{1}{K_L q_L} \cdot \frac{1}{C_e} \tag{4}$$

Where C_e is the equilibrium concentration of adsorbate (mg/L), C_o is the maximum initial concentration (mg/L), q_e the amount of metal ion adsorbed at equilibrium (mg/g), and q_L is the metal ion maximum adsorption (mg/ g) and K_L (L /g) is the Langmuir adsorption equilibrium constant. q_L and K_L are calculated from the slope and intercept of the isotherm plot C_e/q_e vs. C_e.

A dimensionless separation factor (R_L) to describe the favorite nature of the adsorption process was calculated from the following Eq. (5).

$$R_L = \frac{1}{1 + C_o K_L} \tag{5}$$

Value of this parameter can show if the adsorption process is either irreversible ($R_L = 0$), favorable ($0 < R_L < 1$), linear ($R_L = 1$) or unfavorable isotherm ($R_L > 1$).

Freundlich isotherm assumes multilayer surface coverage and heterogeneous adsorption on the adsorbent's surface. The linear form of this empirical model as represented in Eq. (6) [23]:

$$\ln q_e = \ln K_F + 1/n \ln C_e \tag{6}$$

Where K_F (mg/g (L/mg)$^{1/n}$) is roughly an indicator of the adsorption capacity and $1/n$ is the adsorption intensity. Freundlich constants K_F and n can be calculated from the intercept and slope of the linear plot with $\ln q_e$ versus $\ln C_e$. Based on values of 1/n, the adsorption is classified as, a favorable if 1/n is between 0 and 1, ($0 < 1/n < 1$), irreversible when 1/n is 0 and unfavorable when 1/n is greater than 1, ($1/n > 1$).

On application of the Temkin isotherm model, the heat of adsorption was explored and used to explain indirect interactions of the adsorbent with Cr(VI) within a medium range of concentrations (ignoring low and high concentrations) of chromium. In its linear form Temkin equation is represented in Eq. (7) [24];

$$q_e = B \ln KT + B \ln Ce \tag{7}$$

Where K_T (L/g) is the Temkin isotherm constant, q_e (mg/g) is the quantity of Cr(VI) adsorbed at equilibrium; C_e (mg/L) is the equilibrium Cr(VI) concentration of in solution and, B is a constant which relates to heat of adsorption (B = RT/b, R (8.314 J/ mol /K) being the universal gas constant, b is the Temkin constant (J/mol) and T (K) is the absolute temperature.

For simulating the kinetic studies of Cr (VI) adsorption onto prepared samples, two widely used kinetics models; pseudo-first order and pseudo-second order models were used. The equations of both models are expressed as pseudo-fist order model as described by Lagergren [25]:

$$log (q_e - q_t) = log q_e - \left[\frac{k_1}{2.303}\right] t \tag{8}$$

Pseudo-second order model proposed by Ho and Mckay [26]:

$$\frac{t}{q_t} = \frac{1}{k_2 q_e^2} + \left[\frac{1}{q_e}\right] t \tag{9}$$

Where, q_e is the amount of adsorbed per unit gram of adsorbent (mg/g) at equilibrium, while q_t is the amount of adsorbed per unit gram of adsorbent (mg/g) at time t, k_1, and k_2 are the respective model constant on equilibrium time (t).

3 Results and Discussion

3.1 Adsorbents Characteristics

To investigate the external surface morphology of the obtained activated carbon (AC) and Si@AC were taken as an example as depicted in Fig. 2a and b. It can be seen that the surface of AC sample is characterized to be rough. In addition, there are open holes suggesting formation of pores developed on the surface. For Si@AC sample, Si particles doped AC are appeared as layers cover the surface as well as some of them are diffused through pores into the bulk of AC sample (Fig. 2b). The element composition of resulted activated carbons was determined by the EDX analysis as shown in Fig. 3, which describes the proximate content of elements in weight%. All samples contain high content of C and O elements with P in low content. For Si@AC and Si-N@AC, Si and N are found to be distributed on the surface of AC. These results confirm that AC surface was doped successfully by Si and N particles as active sites for attracting with Cr (VI).
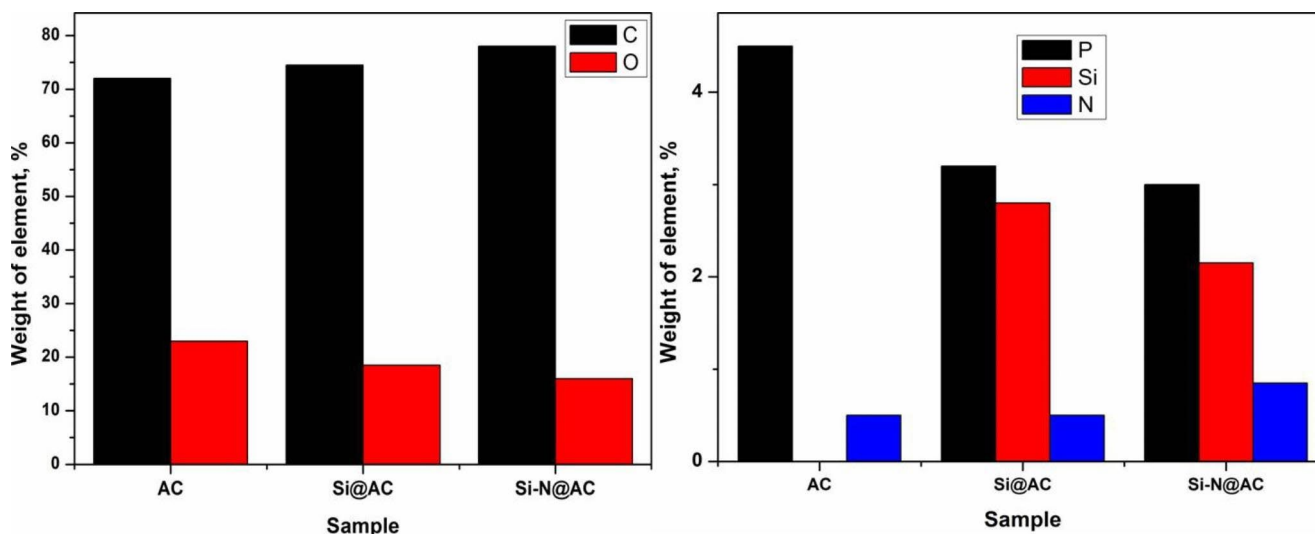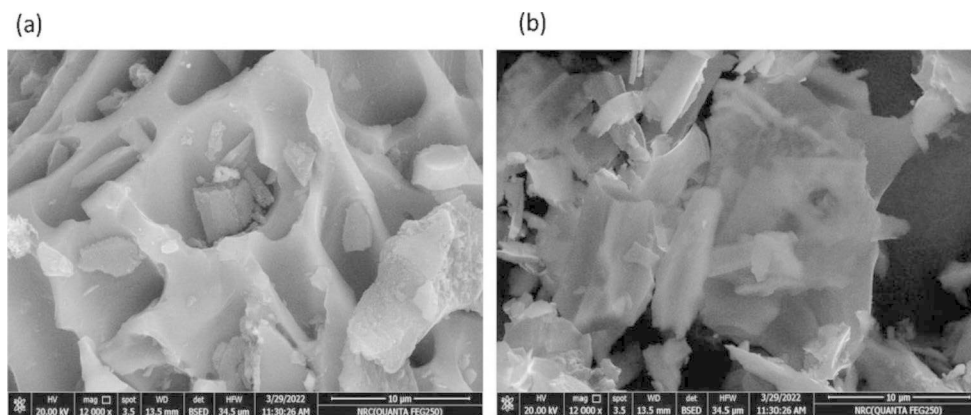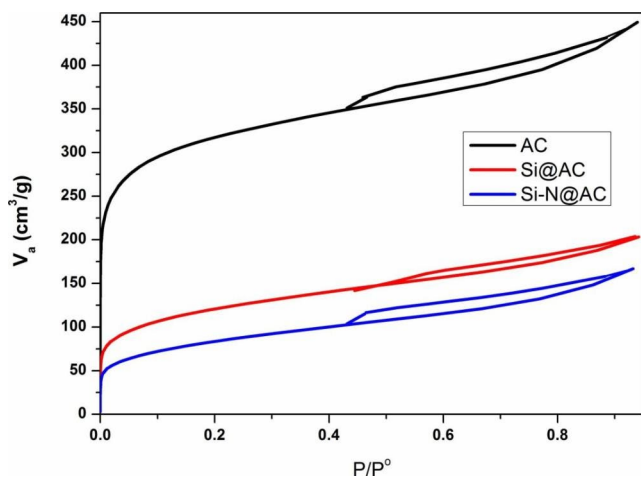
Fig. 2 SEM images of (**a**) AC and (**b**) Si@AC samples

Fig. 3 EDX analysis of element composition in the prepared samples

appears after P/P^o of 0.4. These materials can be categorized as microporous-mesoporous materials. It can be seen also that the origin AC sample showed the highest adsorption of N_2 as compared to other Si@AC and Si-N@AC samples. This finding indicates that the modification of AC surface with Si and N affected the internal porosity of AC samples. Perhaps Si and N retained in the micropores and hence a decrease in both total surface area and pore volume whereas an increase in the mean pore diameter is obtained. Table 1 summarizes the porous characteristics of these samples.

Results of surface pH for obtained samples showed that AC, Si@AC and Si-N@AC possess pH of 4, 4.5 and 6, respectively; as listed in Table 1. Thus the surface of AC is changed from strong acidic to slight acidic in nature confirming the modification of AC surface with non-acidic surface groups related to nitrogen functional surface groups. These changes in such surface groups can be confirmed by FTIR spectra recorded at range $4000-400 \text{ cm}^{-1}$ for the obtained samples as shown in Fig. 5.

Five absorption characteristics bands at the following regions: 3431 cm^{-1}, 2079 cm^{-1}, $1635/1619 \text{ cm}^{-1}$, 1385 and

Fig. 4 Adsorption isotherms of N_2 onto prepared samples

Figure 4 describes the adsorption isotherms of nitrogen onto the samples to detect the porosity development. The adsorption isotherms confirm that the materials prepared are belonging to Type I combined with IV as hysteresis loop

Table 1 Porous characteristics of the prepared samples as accounted from N_2 adsorption at $-196°C$ (Total surface area (S_{BET}, m^2/g), total pore volume (V_P, cm^3/g), mean pore diameter (W_P, nm), α-micropore surface area ($S_{\alpha\, micro}$, m^2/g), and α-micropore volume ($V_{\alpha,\, micro}$, cm^3/g))

Samples	pH	S_{BET} (m^2/g)	V_P (cm^3/g)	W_P (nm)	$S_{\alpha,\, micro}$ (m^2/g)	$V_{\alpha,\, micro}$ (cm^3/g)	$V_{\alpha,\, micro}/V_{P}$, %
AC	4	1220	0.765	2.51	1100	0.588	76.8
Si@AC	4.5	442	0.595	5.85	355	0.382	64.3
Si-N@AC	6	305	0.358	4.69	229	0.196	54.7
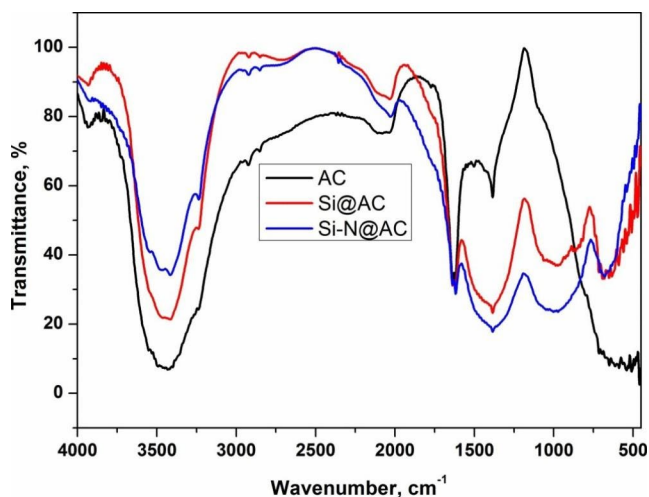
Fig. 5 FTIR spectra of the investigated samples

Fig. 6 Adsorption isotherms of Cr(VI) by the investigated samples

$725-420$ cm^{-1} are observed for the origin AC sample with higher absorbance intensities than that of other two samples. These bands are referred to O-H, H-N, C=C, C=O and C-H out-of-plane stretching in the aromatic rings, respectively [16, 27–29]. After addition of Si particles to surface of AC sample, the absorbance intensity of these bands is decreased with shifting in their wavenumbers (cm^{-1}). Moreover, two broad absorption bands located between 1053 and 983 cm^{-1} are obtained upon modification. This finding is related to formation of both Si–O–Si (siloxane) and C–Si–O stretching vibrations (1053 cm^{-1}) and Si–OH silanol (983 cm^{-1}) [27, 28]. Doping of Si@AC with further N groups led to shifting absorption band at 2079 to 1987 cm^{-1}. This may be assigned to formation of N-H in NH_3 amine vibration which reasons why the surface pH is raised from 4.5 to 6. From FTIR results, the proposed strategy achieved considerable surface changes which gave rise to increase in the adsorption capacity of AC to adsorb Cr(VI) from aqueous solutions as found in the next section.

3.2 Isotherm Adsorption Studies

The isotherm parameters of Cr(VI) adsorption on the resulting samples of AC, Si@AC, and Si-N@AC samples were determined from the linear modeling of experimental data (Fig. 6) from the applied isotherm models in equations of 4, 6 and 7. Table 2 lists the resulting adsorption parameters of

the used models. Adsorption behavior of Cr(VI) by the sample is F-type by AC and Si-N@AC while L-type by Si@AC as shown in Fig. 6 and also R^2 value of each model (Langmuir and Freundlich models). It can be concluded that Si particles could change the surface character of AC sample from heterogeneous to homogeneous property. Therefore, the Cr(VI) adsorption process by AC and Si-N@AC follows the Freundlich model well, otherwise to adsorption by Si@AC (Fig. 7a & b). Figure 7c describes the Temkin isotherm plots for adsorption of Cr(VI) showing that R^2 values were between 0.92 and 0.95.

From Langmuir parameters, the calculated R_L value can describe the adsorption performance, where their values are less than 1, thus the adsorption of Cr(VI) is favorable and reversible on the adsorbents. The b constant of the Temkin model can be stated the adsorption mechanism, where when the value of b constant < 80,000 J/mole (< 80 kJ/mole) [30], thus the adsorption is physisorption. Furthermore, the results of Temkin model reveal that the value of the b constant is < 80 kJ/mole, confirming an evidence that the nature of Cr(VI) adsorption process onto the resulting samples is physical in nature.

The values of monolayer adsorption capacity calculated from Langmuir (q_L, mg/g) were 82, 286 and 233 mg/g for AC, Si@AC and Si-N@AC adsorbents, respectively. The addition of Si enhanced q_L of AC about 3.5 times whereas further addition of N into Si@AC caused a reduction about 18.5%, but still higher than that of origin AC adsorbent. This finding may be pointed out to further reduction in the total surface area from 442 to 305 m^2/g which accompanied by

Table 2 Adsorption parameters calculated from the Langmuir, Freundlich and Temkin isotherms for adsorption of Cr (VI) ions by the samples

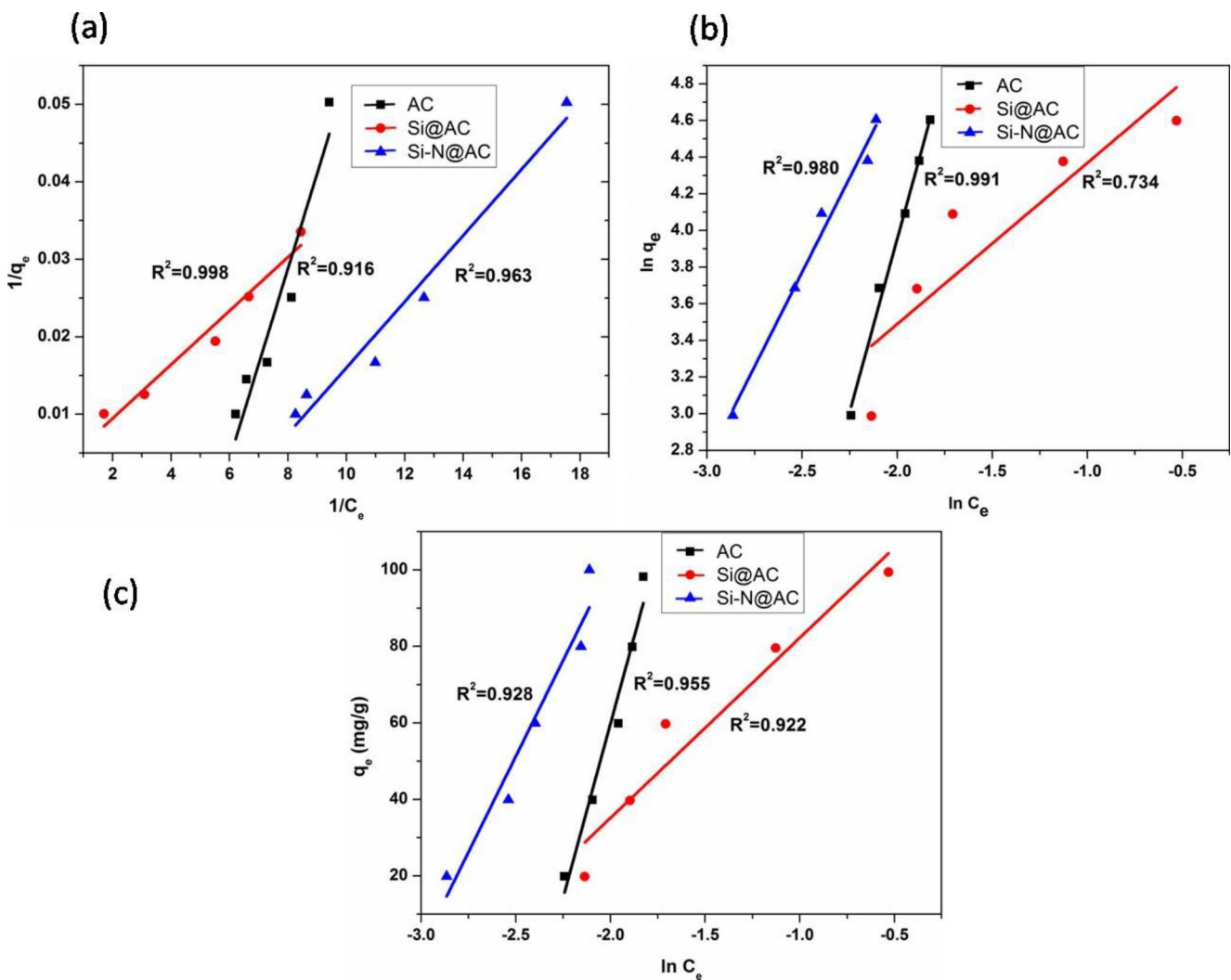| Equilibrium models	Adsorbents		
	AC	Si @AC	Si-N@AC
Langmuir	82	286	233
$q_L (mg/g)$	0.561	0.714	0.604
$K_L (L/g)$	0.017	0.014	0.016
R_L	-22.5	-20.7	-21.8
ΔG	0.916	0.998	0.963
R^2			
Freundlich	74	190	98
$K_F (mg/g\ (L/mg)^{1/n})$	3.77	0.879	2.06
$1/n$	0.991	0.734	0.980
R^2			
Temkin	10.35	15.5	20.3
$K_T (L/mg)$	47	182	100
$B\ (kJ/mol)$	53.8	13.9	25.3
b	0.955	0.921	0.928
R^2			

Fig. 7 Plots of adsorption Cr(VI) ions using (**a**) Langmuir, (**b**) Freundlich and (**c**) Temkin isotherm models

Table 3 Comparison of adsorption capacity of different adsorbents for adsorption of hexavalent chromium at room temperature (25-30ºC)

Adsorbents	Adsorption Capacity (mg/g)	References
Rutin biosorbents	26–41	[3]
Modified palm branch	25	[4]
Extracellular polymeric substances	33.8	[5]
Fox nutshell activated carbon-$ZnCl_2$ activation	43.5	[6]
Activated carbons	16.6–50.4	[7]
Fox nutshell activated carbon-H_3PO_4 activation	75	[8]
Olive bagasse activated carbon	88.5	[9]
sawdust activated carbon	44.05	[10]
Jujuba fruit-activated carbon	126	[11]
Micro-mesoporous activated carbons	24–30	[12]
Goethite-activated carbon composite	6.47	[13]
N-doped porous carbon adsorbent	227.3	[15]
N-doped activated carbon	171.6	[16]
Carbon nanostructures	44–56	[17]
Chitosan grafted graphene oxide	104.2	[18]
Si@AC	268	This study
Si-N@AC	233	This study

Table 4 Adsorption kinetic equation and linear fit parameters for the adsorption of reactive yellow dye onto samples (pH = 2 and T = 30ºC).

Models	Parameter	AC	Si@AC	Si-N@AC
		$C_0 = 100$ mg/L	$C_0 = 100$ mg/L	$C_0 = 100$ mg/L
Pseudo-first-order	$q_{e, exp}$ (mg/g)	87	97	90
	$q_{e,cal}$ (mg/g)	45	66	48
	k_1 (min^{-1})	0.521	0.745	0.845
	R^2	0.645	0.666	0.531
Pseudo-second-order	$q_{e, cal}$ (mg/g)	86	98.2	91
	k_2 (g/mg.min)	0.0216	2.02×10^{-3}	0.026
	R^2	0.999	0.988	0.999

a decrease in the mean pore diameter from 5.85 to 4.69 nm (Table 1). However, the adsorption capacities of Si@AC and Si-N@AC are very higher than that of other adsorbents as shown in Table 3.

The monolayer adsorption capacities (mg/g) of the prepared adsorbents for the removal of Cr(VI) were compared with other adsorbents reported in previous literature as presented in Table 3. It can be concluded that the obtained capacities of the present samples are superior and larger than that of compared samples from the previous literature, affirming the validity of the modification described in this study.

3.3 Kinetic Adsorption Studies

The kinetic studies of Cr (VI) adsorption on the investigated adsorbents were analyzed using linear forms of pseudo-first-order and pseudo-second order models [22–24]. Their corresponding parameters are calculated and summarized in Table 4. The obtained linear plots are displayed in Fig. 8, at initial concentration of Cr(VI) of 100 mg/L and pH of 2 at 30ºC. As seen in Table 4, there is an agreement between the experimental and calculated values of q_e calculated from the pseudo-second order kinetic and the correlation coefficient values (R^2) of this model are close to unity. Accordingly, the pseudo-second-order model is better than the pseudo-first-order model to represent the adsorption of Cr(VI) using the studied samples which governed by a mechanism of chemisorption. Thus, chemical interactions such as electron transfer, ion exchange, or electrostatic binding might occur between the various oxy-anions of Cr (VI) and the radical groups (e.g., -NH- and -COOH) [31, 32]. These findings confirm that the adsorption process may be explained via Van der Waals forces, electrostatic, and H−bonding interactions. As pH value is acidic environment, the protonation of negatively charged sites such as (Si–O–Si), silanol groups (Si–OH), and N-H on the prepared samples can be occurred and formed positively charges of Si–OH^{+2}, for example, that are more suitable to adsorb negatively anions of Cr(VI) through the electrostatic attraction forces. Thereof, the major reaction of the Cr(VI) ions with the functional groups, on the surface of the studied samples, can occur via both physico-chemical adsorption.

3.4 Effect of Temperature on the Biosorption

Three different temperatures (30, 40 and 50ºC) were performed to study the effect of temperature on the adsorption of Cr(VI) on the adsorbent samples and the results are given in Fig. 9. For an increase in temperature from 30 to 50ºC, the adsorption capacities of the samples for Cr(VI) decrease. The decrease in adsorption capacity with increasing temperature indicates an exothermic nature of the adsorption process.

The thermodynamic parameters of Cr(VI) adsorption on the investigated samples, such as enthalpy change ΔHº, free energy change ΔG∘ and entropy change ΔS∘ were calculated using Eqs. [33–35]:

$$\Delta G^0 = --RT \ln K_d \tag{10}$$

$$\ln K_d = \frac{\Delta S^0}{R} - \frac{\Delta H^0}{RT} \tag{11}$$
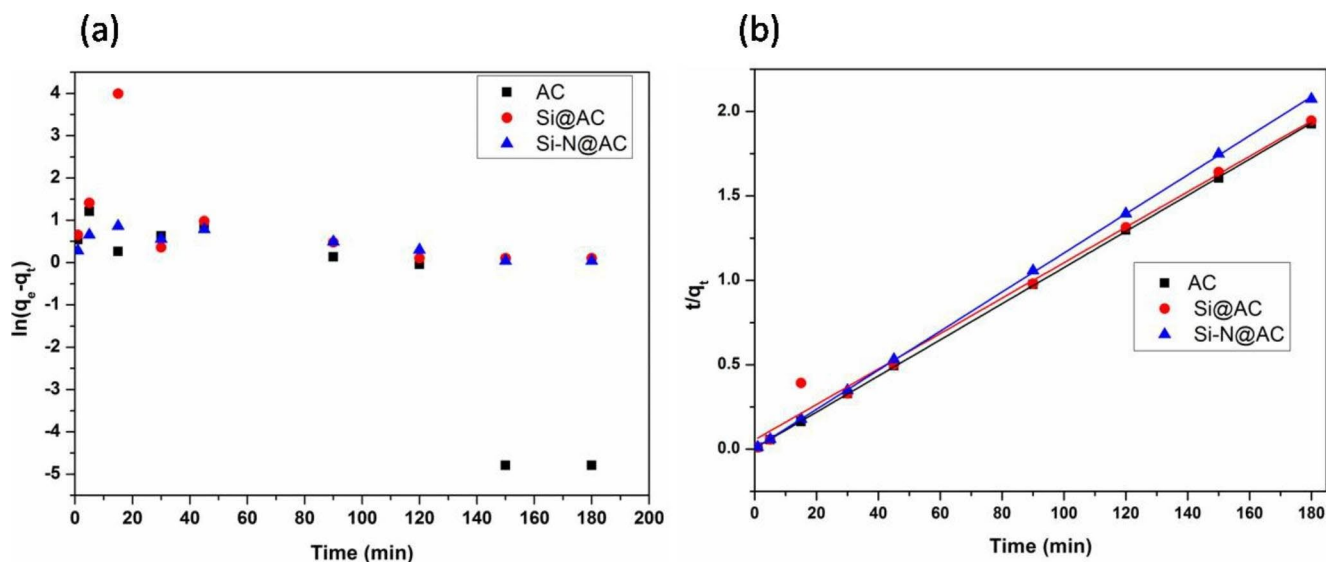
(a)

(b)

Fig. 8 Kinetic plots of Cr(VI) adsorption onto adsorbents using (**a**) pseudo-first-order and (**b**) pseudo-second-order models ($C_o = 100$ mg/L, pH = 2, adsorbent dose = 1 g/1L, contact time = 3 h, and T = 30ºC).
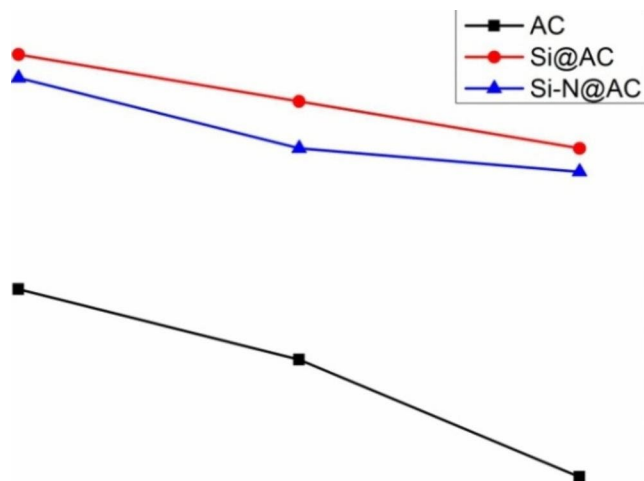

Fig. 9 Effect of temperature on adsorption of Cr (VI) using tested samples

Table 5 Thermodynamic parameters for the adsorption of Cr (VI) at different temperatures

Adsorbent	Temperature (K)	ΔG (kJ/mol))	ΔH(kJ/mol)	ΔS (J/mol K)
AC	303	-33.8	-162.3	− 423.9
	313	-29.6		
	323	-25.7		
Si@AC	303	-30.3	-81.3	-168.5
	313	-28.8		
	323	-27.1		
Si-N@AC	303	-34.8	-157.6	-409.8
	313	-26.5		
	323	-26.7		

where R is the universal gas constant (R = 8.314 J/mol K), T is the absolute temperature (K), and K_d is the distribution coefficient, $K_d = q_e / C_e$ (L/g). From Van't Hoff Eq. (11), the values of ΔH^0 and ΔS^0 were obtained from the slope and intercept of the linear plot of $ln\ K_d$ vs. 1/T (not shown). The values of these parameters are summarized in Table 5. The negative $\Delta G°$ values revealed that the adsorption is thermodynamically feasible and spontaneous nature. It can be seen that values of both enthalpy change $\Delta H°$ and entropy $\Delta S°$ are negative suggesting that the adsorption is exothermic. The negative values indicate the decrease in randomness at the solid–solution interface during the adsorption of the chromium ion on the active sites of the adsorbents. Another evident could describe the mechanism of adsorption; if the value of enthalpy change (ΔH^0) is higher than 40 kJ/mol thus the process is chemisorption including strong electrostatic chemical bonding between chromium ions and adsorbent surface. In this study, the high value of ΔH^0 reveals that the chemisorption controlled the Cr(VI) adsorption on the prepared activated carbon.

4 Conclusions

This research investigated a novel modification to improve the adsorption behavior of Cr (VI) over AC prepared from sugarcane bagasse. AC sample was doped with Si and another doped with Si and N as active sites. The results showed that the successful preparation of Si@AC and Si-N@AC with an excellent morphological characterization was evident from doping with Si and Si-N using SEM-EDX and FTIR tools. The isotherm data can be represented by

the Freundlich isotherm for AC and Si-N@AC, whereas adsorption using Si@AC adsorbent fitted well with Langmuir isotherm. The pseudo-second-order kinetic model well described the adsorption of Cr(VI). In addition, the adsorption mechanism was governed by physical at equilibrium while it exhibited a chemical mechanism kinetically. Here, it could be seen that the doping of AC with Si and Si-N exhibited higher adsorption capacities of 268 and 233 mg/g than that of AC alone, respectively. Thermodynamic studies showed that the adsorption of Cr(VI) onto studied ACs was feasible, spontaneous, and exothermic at 30–50ºC. Therefore, Si@AC and Si-N@AC are very efficient and promising adsorbents to remove high quantity of Cr(VI) from their polluted water.

Declarations

Conflict of Interest The authors declare that they have no known competing financial interests or personal relationships that could have appeared to influence the work reported in this paper.

References

1. Gupta VK, Rastogi A, Nayak A (2010) Adsorption studies on the removal of hexavalent chromium from aqueous solution using a low cost fertilizer industry waste material. J Coll Interf Sci 342:135–141
2. Uysal M, Irfan A (2007) Removal of cr(VI) from industrial wastewaters by adsorption part I: determination of optimum condition. J Hazard Mater 149:482–491
3. Fathy NA, El-Wakeel ST, Abd El-Latif RR (2015) Biosorption and desorption studies on chromium (VI) by novel biosorbents of raw rutin and rutin resin. J Environ Chem Eng 3:1137–1145
4. Shouman MA, Fathy NA, Khedr SA, Attia AA (2013) Comparative biosorption studies of hexavalent chromium ion onto raw and modified palm branches. Adv Phys Chem 2013:1–9
5. Wang H, Wang W, Zhou S, Gao X (2023) Adsorption mechanism of cr(VI) on woody-activated carbons. Heliyon 9:e13267
6. Kumar A, Jena HM (2017) Adsorption of cr(VI) from aqueous phase by high surface area activated carbon prepared by chemical activation with ZnCl₂. Process Safe Environ Protect 109:63–71
7. Fang Y, Yang K, Zhang Y, Peng C, Robledo-Cabrera A, López-Valdivieso A (2021) Highly surface activated carbon to remove cr(VI) from aqueous solution with adsorbent recycling. Environ Res 197:111151
8. Kumar A, Jena HM (2017) Adsorption of cr(VI) from aqueous solution by prepared high surface area activated carbon from Fox nutshell by chemical activation with H₃PO₄. J Environ Chem Eng 5:2032–2041
9. Demiral H, Demiral I, Tümsek F, Karabacakoğlu B (2008) Adsorption of chromium (VI) from aqueous solution by activated carbon derived from olive bagasse and applicability of different adsorption models. Chem Eng J 144:188–196
10. Karthikeyan T, Rajgopal S, Miranda LR (2005) Chromium (VI) adsorption from aqueous solution by Hevea Brasilinesis sawdust activated carbon. J Hazard Mater 124:192–199
11. Labied R, Benturki O, Hamitouche AE, Donnot A (2018) Adsorption of hexavalent chromium by activated carbon obtained from a waste lignocellulosic material (Ziziphus jujuba cores): kinetic, equilibrium, and thermodynamic study. Adsorp Sci Technol 36:1066–1099
12. Ammar NS, Fathy NA, Ibrahim HS, Mousa SM (2021) Micro-mesoporous modified activated carbon from corn husks for removal of hexavalent chromium ions. Appl Water Sci 11:1–12
13. Adebayo GB, Adegoke HI, Fauzeeyat S (2020) Adsorption of cr(VI) ions onto goethite, activated carbon and their composite: kinetic and thermodynamic studies. Appl Water Sci. https://doi.org/10.1007/s13201-020-01295-z.
14. Aggarwal D, Goyal M, Bansal RC (1999) Adsorption of chromium by activated carbon from aqueous solution. Carbon 37:1989–1997
15. Chen F, Guo S, Wang Y, Ma L, Li B, Song Z, Huang L, Zhang W (2022) Concurrent adsorption and reduction of chromium (VI) to chromium(III) using nitrogen-doped porous carbon adsorbent derived from loofah sponge. Front Environ Sci Eng 16(5):57
16. Chu B, Amano Y, Machida M (2020) Preparation of bean dreg derived N-doped activated carbon with high adsorption for cr(VI). Coll Surf A: Physicochem Eng Aspects 586:124262
17. Fathy NA, El-Khouly SM, El-Shafey OI (2021) Modified carbon nanostructures obtained from sugarcane bagasse hydrochar for treating chromium-polluted water. Curr Anal Chem 17:975–988
18. Samuel MS, Bhattacharya J, Raj S, Santhanam N, Singh H, Singh ND (2019) Efficient removal of chromium(VI) from aqueous solution using chitosan grafted graphene oxide (CS-GO) nanocomposite. Int J Biol Macromol 121:285–292
19. Baig N, Chauhan DS, Saleh TA, Quraishi MA (2019) Diethylenetriamine functionalized graphene oxide as a novel corrosion inhibitor for mild steel in hydrochloric acid solutions. New J Chem 43:2328–2337
20. Karthik R, Meenakshi S (2014) Removal of hexavalent chromium ions using polyaniline/silica gel composite. J Water Proc Eng 1:37–45
21. Bilgiç A, Çimen A (2019) Removal of chromium(VI) from polluted wastewater by chemical modification of silica gel with 4-acetyl-3-hydroxyaniline. RSC Adv 9:37403–37414
22. Langmuir I (1918) The adsorption of gases on plane surfaces of glass, mica and platinum. J Am Chem Soc 40:1361–1403
23. Freundlich HMF (1906) Over the adsorption in solution. J Phys Chem 57:385–470
24. Temkin MI, Pyzhev V (1940) Kinetic of ammonia synthesis on promoted iron catalyst. Acta Phys Chem URSS 12:327–356
25. Lagergren S (1898) Zurtheorie der sogenannten adsorption gelosterstoffe. 591. Kungliga Svenska Vetenska psakademiens. Handlingar 24:1–39
26. Ho YS, McKay G (1998) Sorption of dye from aqueous solution by peat. Chem Eng J 70:115–124
27. Fu L, Zhu I, Huang W, Fang J, Sun X, Wang X, Liao K (2020) Preparation of nano-porous carbon-silica composites and its adsorption capacity to volatile organic compounds. Processes 8:372

28. Chatterjee R, Sajjadi B, Chane W, Mattern DL, Hamner N, Raman V, Dorris A (2020) Effect of pyrolysis temperature on physicochemical properties and acoustic-based amination of biochar for efficient CO_2 adsorption. Front Energy Res 8:85

29. Mohamed GM, Rashwan WE, Fathy NA, Ahmed SA (2019) Effect of nitrogen functionalization on the adsorption performance of commercial charcoal activated with phosphoric acid. Desal Water Treat 148:178–187

30. Nasseh N, Khosravi R, Abu Rumman G, Ghadirian M, Eslami H, Khoshnamv M, Al-Musawi TG, Khosravi A (2021) Adsorption of cr(VI) ions onto powdered activated carbon synthesized from Peganum harmala seeds by ultrasonic waves activation. Environ Technol Innov 21:101277

31. Hussain I, Qi J, Sun X, Wang L, Li J (2020) Melamine derived nitrogen doped carbon sheet for the efficient removal of chromium(VI). J Molec Liquids 318:114052

32. Guo C, Ding L, Jin X, Zhang H, Zhang D (2021) Application of response surface methodology to optimize chromium(VI) removal from aqueous solution by cassava sludge-based activated carbon. J Environ Chem Eng 9(1):104785

33. El-Sherif IY, Fathy NA (2013) Modification of the adsorptive characteristics of bagasse fly ash for uptaking cadmium from aqueous solution. Environ Res Eng Manag 2:19–28

34. Singh S, Anil AG, Khasnabis S, Kumar V, Nath B, Adiga V, Naik TS, Subramanian S, Kumar V, Singh J, Ramamurthy PC (2022) Sustainable removal of cr(VI) using graphene oxide-zinc oxide nanohybrid: adsorption kinetics, isotherms and thermodynamics. Environ Res 203:111891

35. Khan MA, Kim S-W, Khan Rao RA, Abou-Shanab RAI, Bhatnagar A, Song H, Jeon B-H (2010) Adsorption studies of dichloromethane on some commercially available GACs: effect of kinetics, thermodynamics and competitive ions. J Hazard Mater 178:963–972